Production and discovery of neutron-rich isotopes by fragmentation of ^{198}Pt

K. Haak,[1,2,*] O. B. Tarasov,[1] P. Chowdhury,[3] A. M. Rogers,[3] K. Sharma,[3] T. Baumann,[1] D. Bazin,[1,2] P. C. Bender,[3] J. Chen,[1] A. Estrade,[4] M. A. Famiano,[5] D. C. Foulds-Holt,[3,†] N. Fukuda,[6] A. Gade,[1,2] T. N. Ginter,[1] R. W. Gohier,[5] M. Hausmann,[1] A. M. Hill,[1,2] D. E. M. Hoff,[3,‡] L. Klankowski,[5] E. Kwan,[1] J. Li,[1] S. N. Liddick,[1,7] B. Longfellow,[1,2,‡] S. Lyons,[1,§] C. Morse,[8] M. Portillo,[1] D. Rhodes,[1,2,‖] A. L. Richard,[1,‡] S. Samaranayake,[4] B. M. Sherrill,[1,2] M. K. Smith,[1] M. Spieker,[1,¶] C. S. Sumithrarachchi,[1] H. Suzuki,[6] K. Wang,[4] S. Waniganeththi,[3] D. Weisshaar,[1] and S. Zhu[9,**]

[1]*Facility for Rare Isotope Beams, Michigan State University, East Lansing, Michigan 48824, USA*
[2]*Department of Physics and Astronomy, Michigan State University, East Lansing, Michigan 48824, USA*
[3]*Department of Physics, University of Massachusetts Lowell, Lowell, Massachusetts 01854, USA*
[4]*Central Michigan University, Mt Pleasant, Michigan 48859, USA*
[5]*Western Michigan University, Kalamazoo, Michigan 49008, USA*
[6]*RIKEN Nishina Center, 2-1 Hirosawa Wako, Saitama 351-0198, Japan*
[7]*Department of Chemistry, Michigan State University, East Lansing, Michigan 48824, USA*
[8]*Nuclear Science Division, Lawrence Berkeley National Laboratory, Berkeley, California 94720, USA*
[9]*National Nuclear Data Center, Brookhaven National Laboratory, Upton, New York 11973, USA*

(Received 27 June 2023; accepted 11 August 2023; published 7 September 2023)

Production cross sections were measured for fragments produced by an 85 MeV/u ^{198}Pt beam incident on a beryllium target. Event-by-event particle identification of A, Z, and q for the reaction products was performed by employing energy loss, time-of-flight, magnetic rigidity, and total kinetic energy measurements. Over 70 nuclei in the Hf-Pt region were identified, including three isotopes first observed in this work: ^{191,192}Hf and ^{189}Lu. Due to the existence of multiple charge states between H-like and C-like ions, a new analysis method was introduced, incorporating Monte Carlo calculations of charge state fractions for a given charge state of the projectile residue just after the reaction. For the first time, charge-state probability distribution functions after the reaction have been deduced from experimental data. This study provides insight into how to produce key nuclides near $N = 126$ and the ability of a fragmentation residue to retain electrons from the primary beam.

DOI: 10.1103/PhysRevC.108.034608

I. INTRODUCTION

The properties of neutron-rich heavy isotopes near the $N = 126$ shell closure are important for our understanding of nuclear physics and play a fundamental role in astrophysical processes such as the r process [1]. Despite their importance, the $N = 126$ isotones for atomic numbers less than lead are poorly studied due to the lack of sufficiently high production cross sections. Only four isotones have been produced and identified over the past few decades [2–5]. In order to establish a footing in this region and eventually reach out toward the location of the r-process pathway and beyond, it is desirable to perform experiments studying the production of neutron-rich isotopes in the Hf-Pt region. This paper describes exploration of the region and identification of new isotopes made from heavy-ion fragmentation.

Previous attempts to produce and study nuclides with $N = 126$ and $Z < 82$ have used a variety of techniques and discovered a number of new isotopes. Other than some limited spectroscopic studies [6] and half-life measurements [7] the past work has mainly aimed to discover new nuclides and measure production cross sections in this region. These studies employed several different reaction mechanisms, including projectile fragmentation [8,9], charge-exchange [4], fission [10], transfer [6], and multinucleon transfer reactions [11]. New isotopes in this region have been produced by fragmentation of ^{238}U [5] and ^{208}Pb [12] beams on beryllium targets at around 1 GeV/u. Multinucleon transfer via low-energy interactions of two high-Z neutron-rich nuclei has been explored as well and indicates promise for much higher production cross sections than fragmentation [13–15]. Despite these efforts, the low production cross sections for nuclei in this region have limited the number of lighter $N = 126$ isotones that could be studied.

This work explores the production of nuclides near $N = 126$ by utilizing projectile fragmentation reactions of beams

*haak@frib.msu.edu
†Present address: University of Cambridge, Cambridge, United Kingdom.
‡Present address: Lawrence Livermore National Laboratory, Livermore, California 94550, USA.
§Present address: Pacific Northwest National Laboratory, Richland, Washington 99352, USA.
‖Present address: TRIUMF, 4004 Wesbrook Mall, Vancouver, BC V6T 2A3, Canada.
¶Present address: Florida State University, Tallahassee, Florida 32306, USA.
**Deceased.

with significantly lower energy than previously employed. Fragmentation production cross sections for nuclei in the $N = 126$ region at intermediate and high energies are modeled by parametrizations and by abrasion-ablation models. EFAX3 [16] is a semiempirical parametrization of fragmentation cross sections, whereas ABRABLA [17,18], COFRA [19,20], and LISE-AA [21,22] are modern versions of the abrasion-ablation model. Two main steps are considered in the abrasion-ablation model: first the projectile-target interaction and second the deexcitation of the products. The cold fragmentation code COFRA is a simplified analytical version of ABRABLA, which only considers neutron evaporation from the prefragments formed in the abrasion stage. The COFRA analytical approach is well suited for extremely low cross sections on the very neutron-rich side, which is difficult to model with the Monte Carlo technique. In this work we concentrate on the fast models EFAX3 and COFRA, which have gained attention for their potential applications in understanding nuclear reactions in various astrophysical and nuclear physics contexts. These models have been extensively employed to explore cross sections across various combinations of projectile-target nuclei, and incident particle energies. EFAX3 has shown promising performance by providing reasonable predictions for the cross sections of projectile fragmentation reactions across a wide range of isotopes close to stability, whereas COFRA has shown some capabilities in describing cross sections in neutron-rich regions [5]. While these models have shown moderate agreement with experimental data over a wide energy range, further investigations and comparisons with recent experimental measurements are necessary to establish their reliability and accuracy in capturing the intricacies of nuclear reactions.

As the neutron-rich region near $N = 126$ is a relatively unexplored frontier, the methods for both production and analysis are not fully developed. At intermediate energies, it becomes increasingly challenging to produce separable and identifiable fragments at increasing atomic numbers due to the inability to fully strip fragments after production. The presence of several charge states in the fragment separator necessitates total kinetic energy (TKE) measurements in order to unambiguously identify each fragment. Even with the ability to measure the charge of each fragment, it is challenging to accurately calculate the exceedingly small charge-state fractions of ions, which lie on the tail end of a charge-state distribution, such as boron-like ions.

In this paper, we will explain the methods of particle identification in this region and demonstrate how they were utilized to identify new isotopes. Additionally, we will outline the difficulties of cross-section analysis in this region, and explore ways of testing underlying assumptions by performing Monte Carlo and analytical simulations of a fragment's path through the separator and all materials traversed.

II. EXPERIMENT

A. Setup

A $^{198}Pt^{61+}$ beam was accelerated by the Coupled Cyclotron Facility (CCF) at the National Superconducting Cyclotron Laboratory (NSCL) at Michigan State University to an energy of 85 MeV/u and an intensity of 0.3 pnA. A combination of the A1900 fragment separator and the S800 analysis beam line was used to separate and identify rare isotopes produced from fragmentation of the ^{198}Pt beam. Both nickel and beryllium targets of varying thickness were utilized and located at the target position of the A1900.

The experimental setup is shown in Fig. 1. This two-stage separation system is similar to our previous experiment with a ^{82}Se beam [24], which allowed for a high degree of rejection of unwanted reaction products. However, in this work the S800 beam-line optics were modified to ensure a 50 mm/% dispersion at the target location of the S800 spectrometer. This modification made it possible to measure momentum without using additional material in the beam line, establishing an optimal configuration for preserving initial charge state distributions of fragments exiting the production target. Momentum selection slits were present at Image 1 of the fragment separator. At the end of the S800 analysis beam line, the particles of interest were stopped in a PIN diode telescope consisting of five silicon detectors (50×50 mm^2), with thicknesses of 140 μm, 140 μm, 500 μm, 1000 μm, and 1000 μm, respectively. A timing scintillator (150 μm) was placed at the focal plane (FP) of the A1900 fragment separator, as shown in Fig. 1.

The signals produced in the telescope detectors were used to perform energy loss and total kinetic energy measurements. The third PIN diode, a single-sided Si strip detector, was used to measure position in the dispersive dimension and therefore reconstruct a momentum to be used for particle identification (PID). The HPGe detector array, GRETINA [23], surrounded the telescope at the end of the S800 analysis beam line and was used to measure γ rays for high-confidence PID via isomer tagging. The delayed timing signal from the scintillator was used as the stop signal for the time of flight (ToF). The timing signal from the first pin in the silicon stack was used as the event trigger and ToF start signal.

B. Experimental procedure

A concern for experiments at intermediate or low energies is the multiple charge states of the beam exiting the production target. In inverse kinematics experiments, various methods are employed to prevent primary beam charge states from reaching the detectors. One approach involves inclining the primary beam on the target, as demonstrated in the case of a ^{238}U beam at 24 MeV/u on light targets at GANIL using the LISE3 fragment separator [25]. Alternatively, thick targets can be utilized to shift the primary beam charge states to a lower magnetic rigidity relative to the fragments of interest. This method has been demonstrated by the BigRIPS separator group in RIKEN experiments [26,27] with a ^{238}U beam at 354 MeV/u. However, with a ^{198}Pt beam at 85 MeV/u using the A1900 separator, neither of these methods could be applied, necessitating the use of a thin target to select fragments at rigidities between the primary beam charge states. Each time a target was replaced, the charge state distribution of the primary beam was mapped out by varying the magnetic rigidity of the first two dipoles of the fragment separator

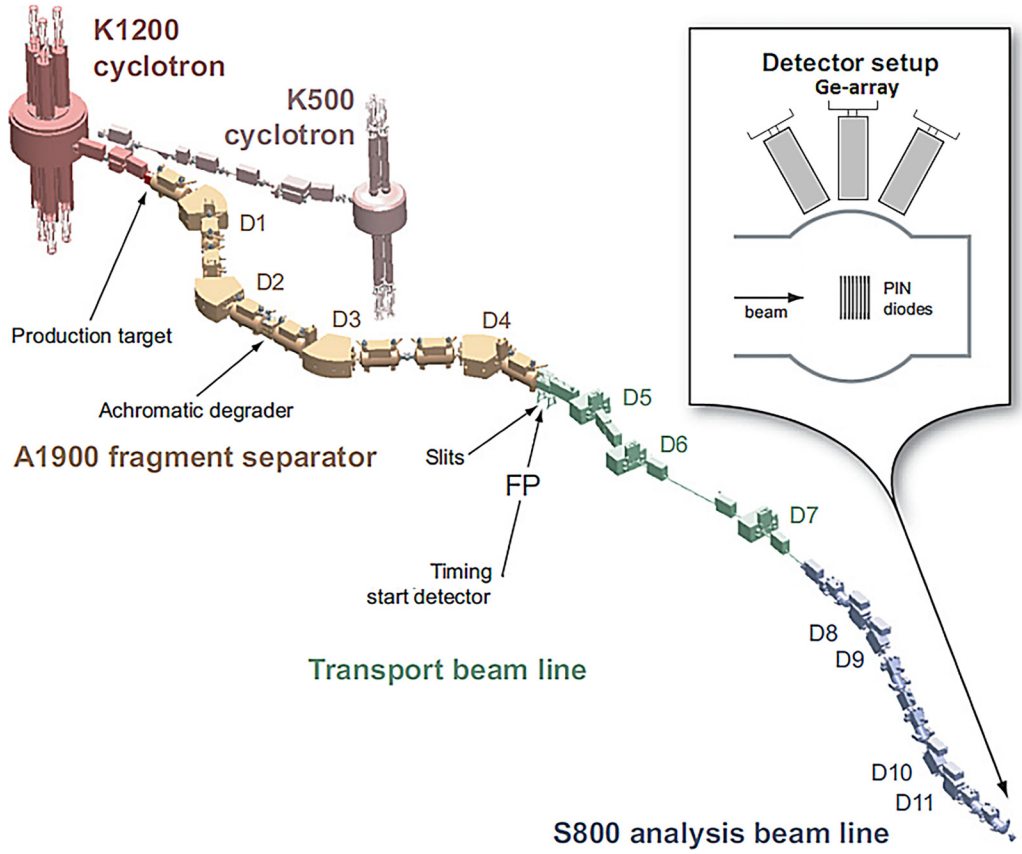

FIG. 1. Sketch of the experimental setup used in the current work. A ^{198}Pt beam was produced by the NSCL coupled cyclotrons and fragmented on a beryllium target at the start of the A1900 fragment separator. Fragments were transported to the target location of the S800 spectrometer and stopped in a silicon telescope surrounded by GRETINA [23].

(D_1, D_2). Therefore, the central $B\rho$ could be set to a value between charge states of the primary beam.

This experiment was comprised of three parts, as listed in Table I. The three objectives were: (i) isomer tagging for PID, (ii) conducting an isomer study, and (iii) the production of new isotopes. The data sets D2, D3, D6a, and D7 were analyzed in this work. In these sets, the only material present after the target was a scintillator at the focal plane of the A1900. For new isotope production, the separator was tuned on more exotic hafnium fragments, namely ^{189}Hf and ^{192}Hf. The wedge was not used at these settings due to the already low detection rate of exotic fragments. It was a priority to maintain a high momentum acceptance while striking a balance between increasing the statistics of reaction products and minimizing detector damage caused by the edge of the primary beam.

TABLE I. Experimental settings.

Data set	Fragment of interest	Magnetic rigidity, $B\rho(Tm)$ D_1D_2	D_3D_4	$D_5D_6D_7$	Target mg/cm^2		Stripper mg/cm^2		Wedge mg/cm^2	$\Delta p/p$ (%)	Time *hours*	Beam particles	Part
D2	^{197}Ir	3.5150	3.5150	3.4390	Be	23		–	–	0.2	5.9	4.93e12	Isomer tagging
D3a	^{186}Hf	3.5127	3.5127	3.4425	Be	23		–	–	0.1	0.4	7.57e11	
D3b	^{186}Hf	3.5127	3.5127	3.4425	Be	23		–	–	0.9	6.3	4.36e11	
D4a	^{186}Hf	3.4928	3.4928	3.4204	Ni	17	Be	9	–	0.2	3.2	7.18e13	Isomer study
D4b	^{186}Hf	3.4928	3.3912	3.3147	Ni	17	Be	9	22.7	0.8	15.4	1.58e14	
D5	^{186}Hf	3.3948	3.2875	3.2063	Be	47		–	22.7	0.7	18.6	2.07e14	
D6a	^{189}Hf	3.4440	3.4440	3.3638	Be	47		–	–	0.5	22.8	1.72e14	Production
D6b	^{189}Hf	3.5420	3.5420	3.3680	Ni	17	Be	9	–	0.9	14.4	2.68e14	of new
D7a	^{192}Hf	3.4910	3.4910	3.4141	Be	47		–	–	0.7	21.9	6.23e14	isotopes
D7b	^{192}Hf	3.4910	3.4910	3.4141	Be	47		–	–	0.9	13.8	3.00e14	

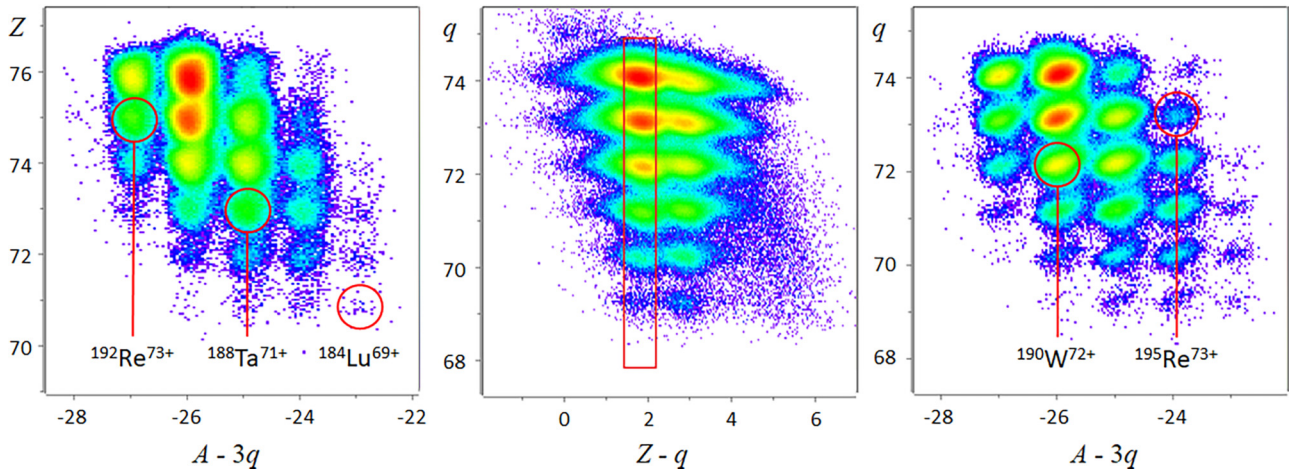

FIG. 2. Particle identification spectra obtained from D4b settings (see Table I). The separation of charge states is demonstrated in the $Z - q$ spectra (center) where helium-like and lithium-like charge states were observed. The charge state selection gate at $Z - q = 2$ (red) is applied to both left and right plots. The Z vs. $A - 3q$ (left) and q vs. $A - 3q$ (right) spectra demonstrate mass, ion charge, and elemental separation quality. A γ-ray spectrum observed in coincidence with $^{190}W^{72+}$ ions labeled here was used to confirm the identification (Fig. 3).

III. ANALYSIS OF EXPERIMENTAL DATA

A. Particle identification

Heavy ions in this study have been identified by the combination of magnetic-rigidity ($B\rho$), time-of-flight (ToF), total kinetic energy (TKE), and energy-loss (ΔE) measurements. The identification of heavy ions using this technique was described in detail in the Appendix of Ref. [28].

The result of using TKE measurements to separate charge states can be seen in the center plot of Fig. 2, which shows the total distribution of charge states observed in the D4b settings of this experiment. The atomic number is denoted by Z, q is the ionic charge, and $A - 3q$ is a calculated quantity proportional to mass. The range of helium-like fragments is shown as both a Z vs. $A - 3q$ spectrum and a q vs. $A - 3q$ spectrum in the left and right plots of Fig. 2, respectively. The confirmation of individual isotopes in Fig. 2 was achieved by isomer tagging the known decays of ^{190}W ($T_{1/2} = 166\,\mu$s) and ^{188}Ta ($T_{1/2} = 3.7\,\mu$s). Figure 3 displays a representative γ-ray spectrum measured with GRETINA [23], which has been gated on ^{190}W (as seen in the right plot of Fig. 2).

B. Production cross section

The production cross section for individual fragments was calculated using the following expression:

$$\sigma = \frac{N_f}{N_b N_t T} \times 10^{27}\,[mb], \tag{1}$$

Where N_f is the number of a given fragment detected at the end of the fragment separator, N_b is the number of total incoming beam particles, T is the transmission of the fragment through the separator, and N_t is the number of target atoms ($1/\text{cm}^2$). N_b is obtained from integrating scaler values that are linearly correlated with beam current, and N_t was derived from the thickness of the target. The fraction of transmitted fragments, T, depends on several factors including the momentum and angular distribution of fragments produced in the reaction, the momentum and angular acceptance of the beams lines, and the charge states populated in the reaction.

The transmission of each fragment was calculated with LISE^{++} (version 16.7) [30,31] using the transmission estimation approach suggested in Ref. [33]. The universal parameterization model was used to calculate the momentum and angular distributions of the fragments. This involves varying several experimental parameters within a reasonable range of uncertainty as listed in Table II. The material thickness, width of momentum slits, and the σ_{conv} and $coef$ parameters of the universal parameterization model [32] were modified to recreate the relative patterns of intensity observed in the experiment. A conservative estimation of error was performed by selecting the maximum, minimum, and mode of all

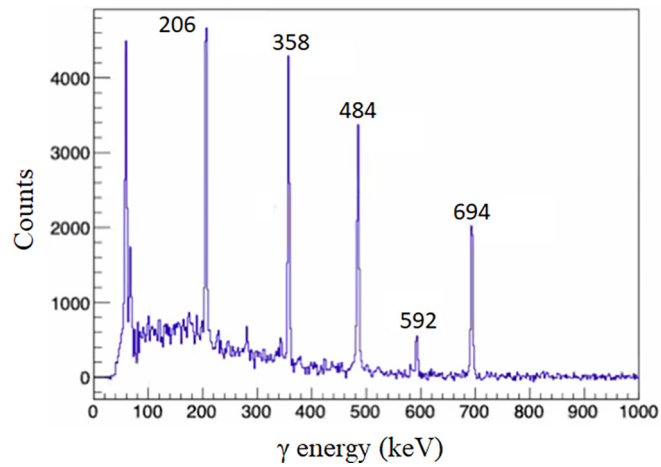

FIG. 3. A γ-ray spectrum of events in GRETINA recorded up to 800 μs after events identified as ^{190}W. The energies of the observed peaks correspond to gamma transitions from the 166 μs isomeric state of ^{190}W [29], confirming particle identification.

TABLE II. Experimental parameters varied to account for uncertainty in transmission. The most probable value for each parameter in each data set is listed. The amount varied is consistent for each data set and is shown in the final column. The target thicknesses listed here are different from what is shown in Table I. This adjustment was made to ensure the best match between experimental transmissions and the given setup in the LISE^{++} code [30,31].

Parameter		D2	D3	D6a	D7	Variation
Beryllium Target (mg/cm^2)		21.80	21.80	50.15	50.15	±2%
Image-1 Momentum Slits (mm)		−2.2 : +2.5	−15.7 : +11.0	−7.7 : +8.0	−10.6 : +10.0	±20%
Momentum Distribution [32]	Width	125	125	125	125	+25
(Separation Energy Model 2)	Coef	0.8	0.8	0.8	0.8	+0.2, −0.3

possible transmission values for a given fragment as the upper error limit, lower error limit, and most probable transmission, respectively.

The yield was calculated via integration of one-dimensional (1D) PID spectra. Gaussian functions were employed to achieve an accurate measurement of the particle yield, even in the presence of neighboring fragments that exhibit overlapping distributions. Each data set was split up into a series of one-dimensional Z spectra and was fit with a series of integer-spaced fixed-width Gaussian functions.

C. Charge-state distributions

The charge-state distributions of reaction products as they exit the production target and traverse subsequent materials is an important factor to consider in the production of high-Z nuclei at intermediate energies. The number of electrons present in the projectile-residue orbitals immediately after a reaction (Ne_R) may influence the charge-state distributions in targets thinner than the equilibrium thickness. Equilibrium target thicknesses for representative ions are given in Table III.

The thicknesses of the targets used in this experiment are significantly below the estimated equilibrium thickness for the high-Z ions of interest. This is demonstrated in Table III, where a variety of charge-state models are considered. The model GLOBAL, which has been incorporated for transmission analysis in the LISE^{++}code, was employed in the further analysis of this experiment. As indicated in the table, GLOBAL estimates an equilibrium thickness around 135 mg/cm^2, whereas the thinnest target used in experiment was 23 mg/cm^2. These calculations explore equilibrium thickness as a function of both atomic number and Ne_R. It is reasonable to assume the charge-state fractions measured in this work contain some information about Ne_R because equilibrium of the charge-state distribution was not reached, and therefore should be considered in this analysis. This makes Ne_R an observable in this experiment.

The presence of nonequilibrium charge states has been confirmed by Monte Carlo calculations of charge state versus reaction place in the target. Figure 4 shows that when $Ne_R = 7$, a substantial number of ions exit the target with high-lying charge states up to $Z - q = 7$ (4.4% of total). Additionally, these ions were produced toward the end of the target. In the case $Ne_R = 0$ (not shown), $Z - q = 0, 1, 2$ charge states dominate, and the $Z - q = 4$ charge state does not exceed 0.1% of the total fraction. Therefore, charge-state distributions are dependent on Ne_R at this thickness. It is important to note that while the primary beam entered the production target with 17 electrons, the prereaction charge state of the primary beam was not taken into consideration for calculations shown in Fig. 4. However, ETACHA4 calculations for the primary beam indicate that, after passing through half the thickness simulated in Fig. 4, the mean charge state $\langle q \rangle$ is estimated to be 73.0 ± 1.4. Ne_R is normally assumed to be zero and the fully stripped ion then picks up electrons as it moves though the target and eventually exits, but in this analysis Ne_R was explored up to a value of seven electrons.

The LISE^{++} code was modified to include Ne_R as a parameter in Monte Carlo calculations of transmission. The default reduction of transmission due to ionization in material for

TABLE III. Equilibrium thicknesses (mg/cm^2) for the charge-state fractions of two representative nuclei produced in this experiment were calculated by several models. An initial energy of 85 MeV/u was used, and the influence of Ne_R on equilibrium thickness was considered.

Model	Ion	^{197}Ir^{70+}	^{197}Ir^{77+}	^{192}Hf^{65+}	^{192}Hf^{72+}
	Ne_R	7	0	7	0
CHARGE [34]		235.9		220.6	
P. Thieberger [35]		108.3		120.8	
GLOBAL [34]		131.3		138.29	
ETACHA4.V3 [36,37]		60.6	65.9	60.9	105.9
ETACHA4.V4 [36,37]		73.6	76.7	75.6	104.1

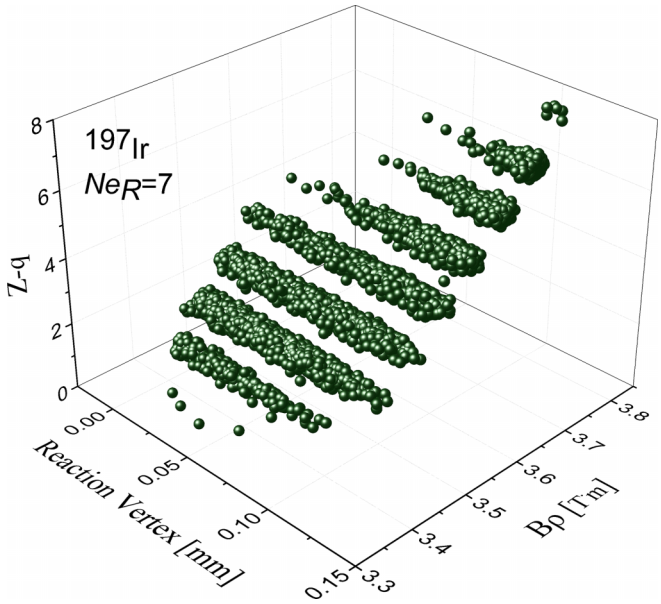

FIG. 4. LISE^{++} 3D Monte Carlo calculations of the charge-state distribution for ^{197}Ir versus the depth in the target at which the reaction occurs, assuming postreaction charge state is $Z - q = 7$. The charge-state model GLOBAL was used.

each ion was removed and then replaced by the reduction factor obtained from the modified Monte Carlo calculation. It was assumed that only fragments that maintained their charge state after exiting the target and passing through subsequent materials, such as the scintillator, would be transmitted to the pin-diode telescope.

A probability distribution function (PDF) of the most likely Ne_R values was constructed for each element and used to deduce production cross sections. The upper bound of the Ne_R domain was set by exploring the functional dependency of the Monte Carlo derived transmission (T) on the Ne_R parameter. The PDF was derived from a χ^2 whose value was determined by three separate considerations: (i) agreement of cross-section measurements between ions of the same nuclei, (ii) physically possible cross-section measurements, and (iii) the continuity of production cross sections for a given isotopic chain as a function of mass. Finally, the experimental cross sections were calculated using a weighted average of all possible outcomes, where the PDF was used for the weights.

IV. RESULTS AND DISCUSSION

A. New isotopes

During the course of the experiment and the measurement of production cross sections, three new isotopes, namely ^{189}Lu and ^{191,192}Hf, were discovered. The evidence for these new isotopes is shown in Fig. 5. Counts to the right of the blue dashed line indicate previously undiscovered nuclides. The measured cross sections of these nuclides were found to be 0.037(24), 0.13(5), and 0.061(44) nb, respectively. These discoveries push the limit of Hf isotopes up to the point where the

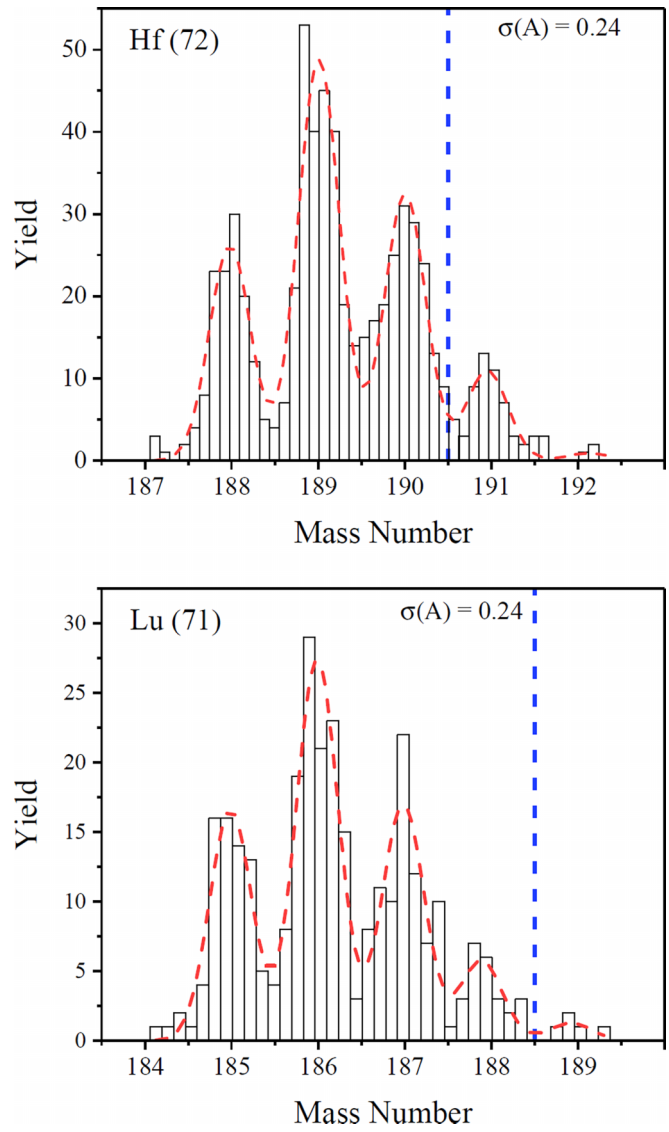

FIG. 5. Mass spectra of hafnium and lutetium isotopes produced in the D7 settings of this experiment. Standard deviations produced with Gaussian functions at constant width (dashed red line) are given for each element. The dashed vertical blue line shows the limit of previously discovered isotopes for each element. The counts at $A = 189$ for $Z = 71$ and $A = 191,192$ for $Z = 72$ are evidence for the discovery of new isotopes.

production of heavier isotopes would involve the pick up of neutrons from the target. Although the experimental settings allowed for the potential observation of new isotopes down to ^{181}Er, they were not detected. This is discussed further in Sec. IV C.

B. Charge states

Not all high-Z fragmentation products at intermediate energies are necessarily formed as fully stripped ions ($Ne_R = 0$), and there may be a correlation between the number of protons removed during the reaction and the number of residual electrons immediately after. This suggestion is grounded in

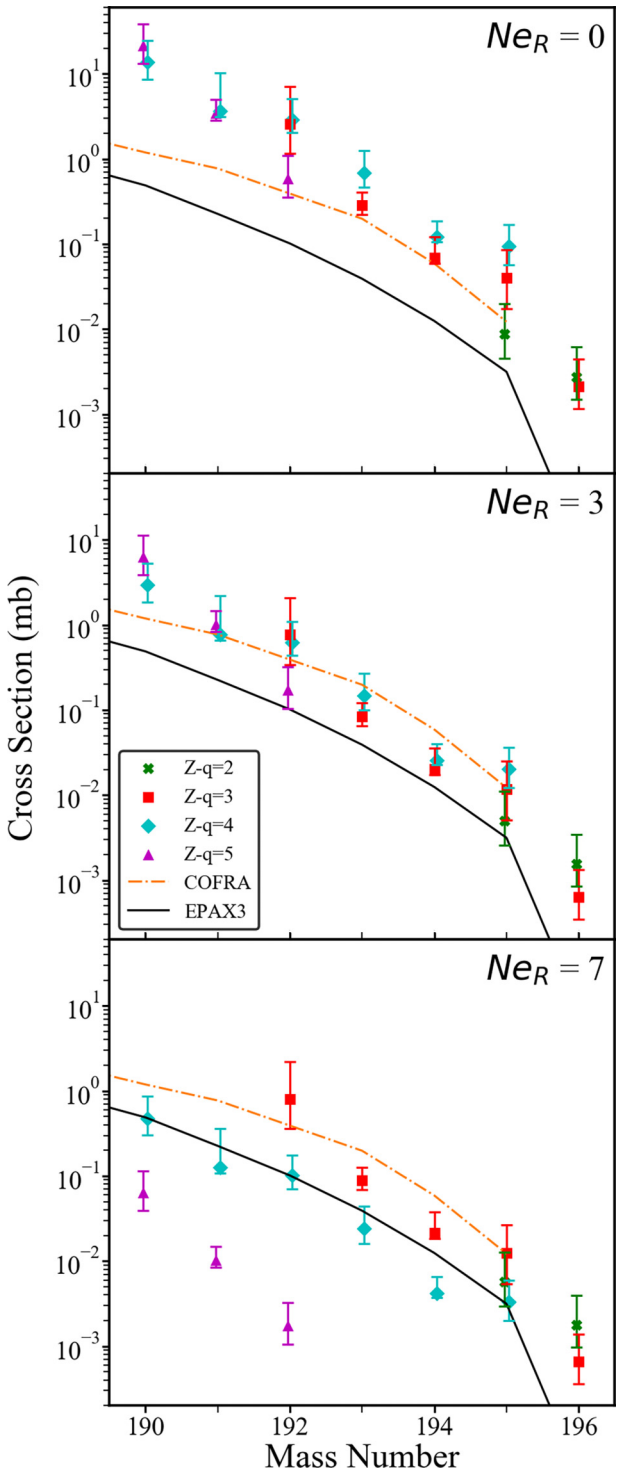

FIG. 6. The cross sections of rhenium isotopes ($Z = 75$), deduced for different values of Ne_R (0,3,7) and separated by charge state, are compared. The cross sections presented here were determined with yields measured in the 47 mg/cm^2 Be target settings. When produced fully stripped ($Ne_R = 0$), the cross-section results for boron-like and beryllium-like ions with nucleon numbers 190 and 191 are extremely large. However, if all fragments are assumed to be produced with seven electrons, the cross sections for boron-like ions appear significantly lower and disjointed from the rest of the data.

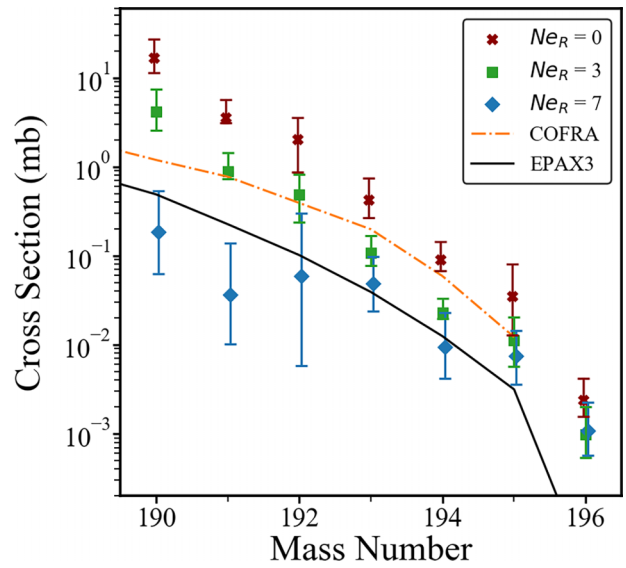

FIG. 7. The cross sections of rhenium isotopes ($Z = 75$), calculated by an error-weighted average of the possible outcomes shown in Fig. 6.

the following observation: ions that lose fewer protons in fragmentation are closer in ionization energy to the original projectile and undergo smaller changes in velocity relative to the projectile. Consequently, there is support for the assumption that the likelihood of electron shake-off following a collision is reduced for cases with less proton removal. The probabilities of electron shake-off resulting from nuclear charge change and nuclear recoil in shaking processes can be derived using the nonrelativistic hydrogenic wave functions [38]. This study indicates that indeed the probability of shake off increases with larger proton removal.

A novel approach to charge-state analysis was developed to accommodate extreme results of cross-section measurements. The choice of Ne_R values was bounded in this work by exploring the parameter space of Ne_R up to seven electrons. Under the assumption $Ne_R = 0$, cross-section calculations produced nonphysical results for certain isotopes, such as cross-section measurements multiple orders of magnitude greater than reasonable model predictions (Fig. 6, top plot). However, assuming $Ne_R = 7$, the cross sections of certain isotopes deduced for different charge states exhibit variations of several orders of magnitude, as evident from the bottom plot of Fig. 6. By comparing the plots in Fig. 6, the optimal solution appears to lie around $Ne_R = 3$ for rhenium isotopes. This conclusion is summarized in Fig. 7 where an error-weighted average of charge states was performed on the data from Fig. 6. Results for mass number 190 and 191 demonstrate the $Ne_R = 0$ assumption is not the most likely. The large variation between underlying charge states for $Ne_R = 7$ leads to very large errors and a discontinuous trend, also indicating a low likelihood for $Ne_R = 7$.

Figure 8 presents the most probable value of Ne_R for each element (Z), obtained for both beryllium targets. This figure demonstrates a prominent trend. More protons removed in a fragmentation reaction corresponds to fewer

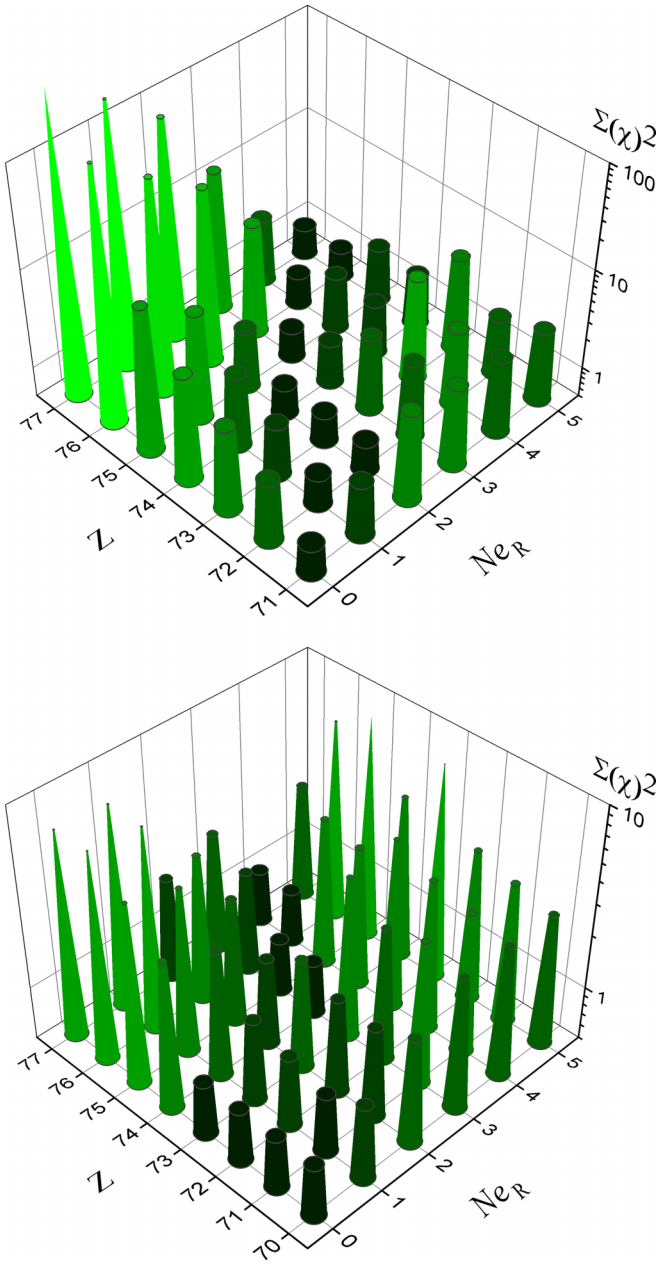

FIG. 8. A summary of the most probable Ne_R values are presented for several elements (Z), derived from the analysis of experimental data. Two different target thicknesses are shown: 23 mg/cm^2 on the top and 47 mg/cm^2 on the bottom. The vertical color axis represents a combination of three optimization considerations: agreement of cross section measurements between ions of the same nuclei, physically possible cross sections measurements, and the continuity of the production cross section for a specific element as a function of nucleon number.

residual electrons on the resulting fragment product. Fragments with higher Z values, which have ionization energies closer to that of the primary beam, tend to retain more electrons compared to lower Z nuclei that are closer to fully stripped ions after fragmentation. This phenomenon can possibly be explained by the fact that fragments with less proton removal have undergone a less violent fragmentation reaction, thereby preserving a greater number of electrons (less shake-off) from the original projectile, $^{198}Pt^{61+}$. This relationship is less pronounced for a thicker target, as the charge state distributions tend to approach equilibrium. Probability distribution functions were derived from this data by normalizing the minimum χ^2 to 1 and then performing an inverse exponential transformation. The base of the exponent was adjusted until the standard deviation of Ne_R was roughly one electron.

C. Cross-section measurements

Using PDFs derived from Fig. 8, the production cross sections were obtained for a total of 60 nuclei in this experiment and are shown in Fig. 9. Details are available as the singular text file in the Supplemental Material [39]. Experimental cross sections follow trends predicted by EFAX3 and COFRA models. However, there is a slight deviation away from the models for lower Z, where the measured cross section is lower than predicted. This effect possibly appears in an odd-even pattern, where the cross sections of isotones with an even number of neutrons are often much lower than their odd counterparts.

No fragments with atomic number (Z) below 70 were produced in significant quantities at the rigidity settings employed in the experiment. Initially, the contribution of the break-up channel in terms of the abrasion-ablation model can explain this phenomenon, where the temperature of the excited prefragment exceeds the limiting temperature [40,41]. However, a more detailed analysis using the LISE-AA [21] model will be conducted to investigate this further. This study of reaction mechanism will also encompass the data involving the Ni-target settings, which is not discussed in this work.

V. SUMMARY

The present study of fragmentation of a ^{198}Pt beam at 85 MeV/u found evidence for three previously unobserved neutron-rich nuclides: ^{192}Hf, ^{191}Hf, and ^{189}Lu. A novel approach was developed to measure cross sections when working with multiple charge states of high-Z fragments. Based on experimental data, the charge-state probability distribution functions (PDF) after the reaction were obtained for a selection of elements, ranging from $Z = 70$ to 77. This is the first time such information has been deduced from experimental data. An evident trend between number of protons removed in a fragmentation reaction and residual electrons was observed, where less proton removal corresponds to more residual electrons in the resulting fragment product. Using charge-state PDFs, production cross sections for 60 nuclei were determined with a beryllium target, and these results were compared with cross-section models. The results are in reasonable agreement with the COFRA parametrization but fall off faster with increasing nucleon removal.

ACKNOWLEDGMENTS

The authors are thankful for the fruitful discussions held with Prof. M. Thoennessen in manuscript preparation. This

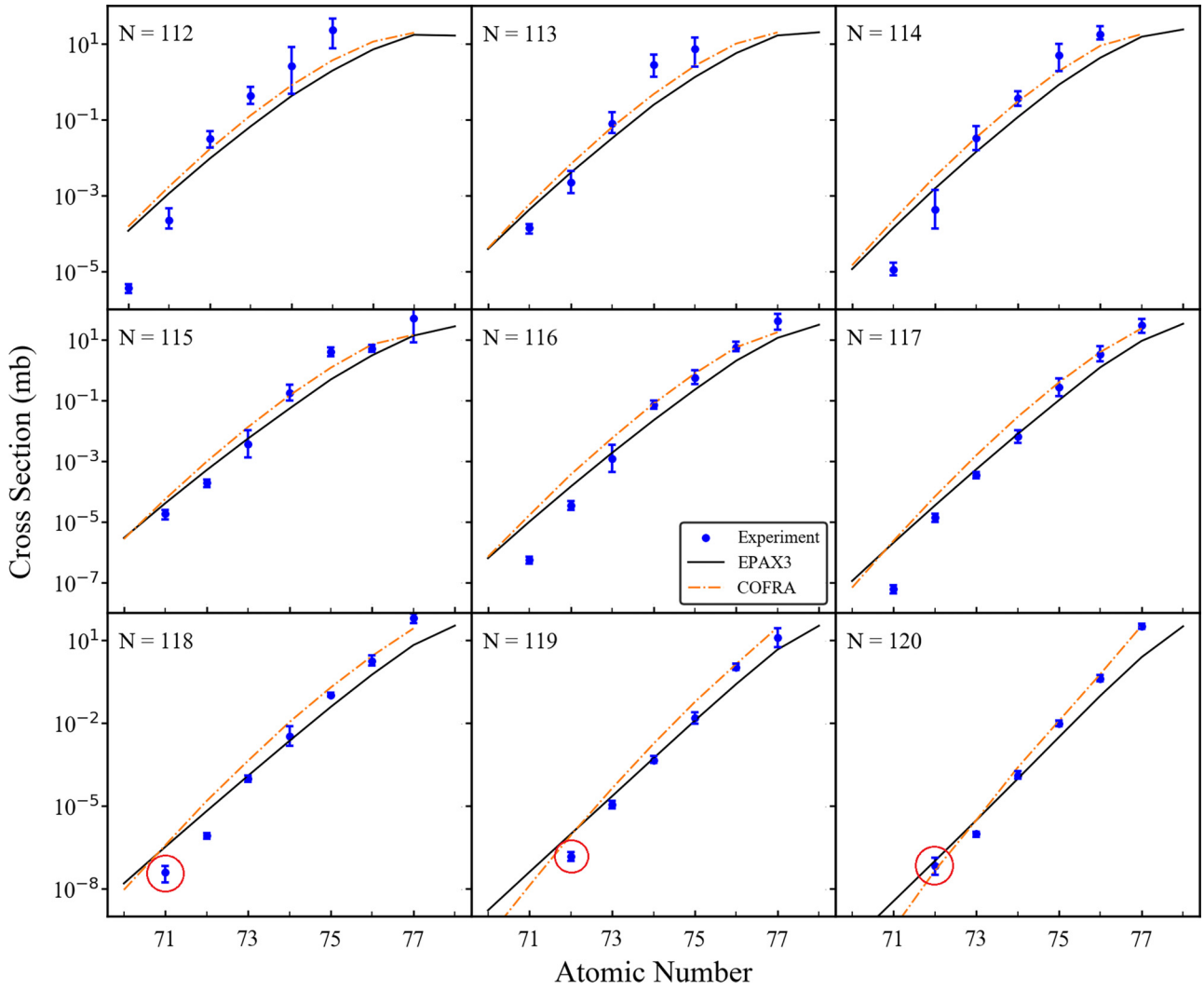

FIG. 9. Cross-section measurements of isotones ($N = 112$–120) as a function of atomic number, produced in the fragmentation reaction of ^{198}Pt (85 MeV/u) with ^{9}Be, are compared to EPAX3 and COFRA calculations. New isotopes are denoted with red circles.

experiment was performed at the NSF's National Superconducting Cyclotron Laboratory (NSCL). The expertise of NSCL operations staff and of the A1900 separator group is gratefully acknowledged. This work was supported by the US National Science Foundation under Grants No. PHY-20-12040 and No. PHY-15-65546 (MSU). This work was also supported by the U.S. Department of Energy, Office of Science, Office of Nuclear Physics, under Awards No. DE-FG02-94ER40848 (UM Lowell), No. DE-AC02-98CH10886 (BNL), No. DE-SC0022538 (CMU), and No. DE-SC0023633 (MSU). GRETINA was funded by the U.S. DOE, Office of Science, Office of Nuclear Physics under Contract No. DE-AC02-05CH11231 (LBNL). This work was also performed under the auspices of the U.S. Department of Energy by Lawrence Livermore National Laboratory under Contract No. DE-AC52-07NA2734.

[1] E. M. Burbidge, G. R. Burbidge, W. A. Fowler, and F. Hoyle, Rev. Mod. Phys. **29**, 547 (1957).

[2] C. Wennemann, W.-D. Schmidt-Ott, T. Hild, K. Krumbholz, V. Kunze, F. Meissner, H. Keller, R. Kirchner, and E. Roeckl, Z. Phys. A **347**, 185 (1994).

[3] S. J. Steer, Z. Podolyák, S. Pietri *et al.*, Phys. Rev. C **78**, 061302 (2008).

[4] A. I. Morales, J. Benlliure, J. Agramunt, A. Algora, N. Alkhomashi, H. Alvarez-Pol, P. Boutachkov, A. M. Bruce, L. S. Caceres, E. Casarejos, A. M. DenisBacelar, P. Doornenbal, D. Dragosavac, G. Farrelly, A. Gadea, W. Gelletly, J. Gerl, M. Gorska, J. Grebosz, I. Kojouharov, F. Molina, D. Perez-Loureiro, S. Pietri, Z. Podolyak, P. H. Regan, B. Rubio, H. Shaffner, S. J. Steer, S. Tashenov, S. Verma, and H. J. Wollersheim, Phys. Rev. C **84**, 011601(R) (2011).

[5] J. Kurcewicz, F. Farinon, H. Geissel *et al.*, Phys. Lett. B **717**, 371 (2012).

[6] T. L. Tang, B. P. Kay, C. R. Hoffman *et al.*, Phys. Rev. Lett. **124**, 062502 (2020).

[7] T. Kurtukian-Nieto, J. Benlliure, K.-H. Schmidt *et al.*, Eur. Phys. J. A **50**, 135 (2014).

[8] T. Enqvist, W. Wlazło, P. Armbruster *et al.*, Nucl. Phys. A **686**, 481 (2001).

[9] T. Enqvist, P. Armbruster, J. Benlliure *et al.*, Nucl. Phys. A **703**, 435 (2002).

[10] M. Albertsson, B. G. Carlsson, T. Døssing, P. Möller, J. Randrup, and S. Åberg, Eur. Phys. J. A **56**, 46 (2020).

[11] O. Beliuskina, S. Heinz, V. Zagrebaev, V. Comas, C. Heinz, S. Hofmann, R. Knöbel, M. Stahl, D. Ackermann, F. P. Heßberger, B. Kindler, B. Lommel, J. Maurer, and R. Mann, Eur. Phys. J. A **50**, 161 (2014).

[12] T. Kurtukian-Nieto, J. Benlliure, K.-H. Schmidt, L. Audouin, F. Becker, B. Blank, E. Casarejos, F. Farget, M. Fernández-Ordóñez, J. Giovinazzo, D. Henzlova, B. Jurado, J. Pereira, and O. Yordanov, Phys. Rev. C **89**, 024616 (2014).

[13] Y. X. Watanabe, Y. H. Kim, S. C. Jeong *et al.*, Phys. Rev. Lett. **115**, 172503 (2015).

[14] V. V. Desai, A. Pica, W. Loveland, J. S. Barrett, E. A. McCutchan, S. Zhu, A. D. Ayangeakaa, M. P. Carpenter, J. P. Greene, T. Lauritsen, R. V. F. Janssens, B. M. S. Amro, and W. B. Walters, Phys. Rev. C **101**, 034612 (2020).

[15] T. Niwase, Y. X. Watanabe, Y. Hirayama *et al.*, Phys. Rev. Lett. **130**, 132502 (2023).

[16] K. Sümmerer, Phys. Rev. C **86**, 014601 (2012).

[17] J.-J. Gaimard and K.-H. Schmidt, Nucl. Phys. A **531**, 709 (1991).

[18] A. Kelić, M. V. Ricciardi, and K.-H. Schmidt, *Proceedings of the Joint ICTP-IAEA Advanced Workshop on Model Codes* (IAEA INDC, 2008), pp. 181–221.

[19] J. Benlliure, K. H. Schmidt, D. Cortina-Gil, T. Enqvist, F. Farget, A. Heinz, A. R. Junghans, J. Pereira, and J. Taieb, Nucl. Phys. A **660**, 87 (1999); **674**, 578 (2000).

[20] J. Benlliure and K. H. Schmidt, References therein; COFRA web page, http://www.usc.es/genp/cofra, Universidade de Santiago de Compostela.

[21] O. B. Tarasov, References therein; LISE^{++} abrasion-ablation web page, https://lise.nscl.msu.edu/AA, Michigan State University.

[22] A. Kubiela, H. Suzuki, O. B. Tarasov, M. Pfützner *et al.*, Phys. Rev. C **104**, 064610 (2021).

[23] S. Paschalis, I. Lee, A. Macchiavelli *et al.*, Nucl. Instrum. Meth. Phys. Res. A **709**, 44 (2013).

[24] O. B. Tarasov, M. Portillo, D. J. Morrissey *et al.*, Phys. Rev. C **87**, 054612 (2013).

[25] O. B. Tarasov, O. Delaune, F. Farget, D. J. Morrissey *et al.*, Eur. Phys. J. A **54**, 66 (2018).

[26] N. Fukuda, T. Kubo, D. Kameda *et al.*, J. Phys. Soc. Jpn. **87**, 014202 (2018).

[27] H. Suzuki, K. Yoshida, N. Fukuda *et al.*, Phys. Rev. C **102**, 064615 (2020).

[28] O. B. Tarasov, M. Portillo *et al.*, Phys. Rev. C **80**, 034609 (2009).

[29] Z. Podolyák, P. Regan, M. Pfützner *et al.*, Phys. Lett. B **491**, 225 (2000).

[30] O. B. Tarasov and D. Bazin, Nucl. Instrum. Meth. Phys. Res. B **266**, 4657 (2008), https://lise.nscl.msu.edu.

[31] O. B. Tarasov and D. Bazin, Nucl. Instrum. Meth. Phys. Res. B **376**, 185 (2016).

[32] O. Tarasov, Nucl. Phys. A **734**, 536 (2004).

[33] O. B. Tarasov, D. Bazin, T. Baumann, A. Gade, T. N. Ginter, M. Hausmann, D. J. Morrissey, J. Pereira, M. Portillo, B. M. Sherrill, A. Stolz, and M. Thoennessen, Nucl. Instrum. Methods Phys. Res., Sect. A **620**, 578 (2010).

[34] C. Scheidenberger, T. Stöhlker, W. Meyerhof, H. Geissel, P. Mokler, and B. Blank, Nucl. Instrum. Meth. Phys. Res. B **142**, 441 (1998).

[35] P. Thieberger, H. E. Wegner, J. Alonso, H. Gould, C. Munger, R. Anholt, and W. E. Meyerhof, IEEE Trans. Nucl. Sci. **32**, 1767 (1985).

[36] E. Lamour, P. D. Fainstein, M. Galassi, C. Prigent, C. A. Ramirez, R. D. Rivarola, J.-P. Rozet, M. Trassinelli, and D. Vernhet, Phys. Rev. A **92**, 042703 (2015).

[37] O. B. Tarasov, D. Bazin, M. Hausmann, M. P. Kuchera, P. N. Ostroumov, M. Portillo, B. M. Sherrill, K. V. Tarasova, and T. Zhang, Nucl. Instrum. Meth. Phys. Res. B **541**, 4 (2023).

[38] P. Sharma, Nucl. Phys. A **968**, 326 (2017).

[39] See Supplemental Material at http://link.aps.org/supplemental/10.1103/PhysRevC.108.034608 for a comma separated text file containing cross section measurements.

[40] J. Besprosvany and S. Levit, Phys. Lett. B **217**, 1 (1989).

[41] Z. Li and M. Liu, Phys. Rev. C **69**, 034615 (2004).